To cite this version :

Justin DIRRENBERGER, Eric MONTEIRO, Nicolas RANC - Representative volume element size determination for viscoplastic properties in polycrystalline materials - International Journal of Solids and Structures - Vol. 158, p.210-219 - 2019

Representative volume element size determination for viscoplastic properties in polycrystalline materials

S. Yang, J. Dirrenberger*, E. Monteiro, N. Ranc

PIMM laboratory, Arts et Métiers ParisTech, Cnam, CNRS, Paris 75013, France

A B S T R A C T

The size of representative volume element (RVE) for 3D polycrystalline material is investigated. A statistical RVE size determination method is applied to a Voronoi tessellation-based pure copper microstructure. The definition of RVE has remained problematic in the literature for properties related to nonlinear viscoplastic behavior, e.g. apparent viscoplastic parameter, intrinsic plastic dissipation. Computational homogenization for elastic and plastic properties is performed within a crystal plasticity finite element framework, over many realizations of the stochastic microstructural model, using periodic boundary conditions. The generated data undergoes statistical treatment, from which RVE sizes are obtained. The method used for determining RVE sizes was found to be operational, even for viscoplasticity. The microscale analysis of the full-field simulation results reveals microstructure-relate heterogeneities which shed new light on the problem of RVE size determination for nonlinear properties.

1. Introduction

In the past decades, full-field numerical simulation of polycrystalline materials based on finite element analysis has been widely developed to investigate the mechanical behavior, allowing the analysis of stress and strain fields at a scale that is not easily assessable experimentally (Barbe et al., 2001; Roters et al., 2011). Most of the authors in the literature dedicated to the simulation of polycrystals usually consider a population of virtual polycrystalline samples made of several hundred grains, validating this arbitrary choice by analyzing the mean value and standard deviation for a given property computed on such population (Shenoy et al., 2007, 2008; Robert et al., 2012; Martin et al., 2014; Sweeney et al., 2015; Cruzado et al., 2017, 2018). Nevertheless, the development of full-field simulation of polycrystalline materials results in shedding new light on the relationship between the microstructural description at the dislocation or grain scale and the local mechanical behavior (Cailletaud et al., 2003a). The homogenized macroscopic response of a polycrystalline material sample will depend on its size, hence yielding the question of representativity for such virtual samples. To bring an answer to this question, one must have a proper definition of what an RVE is.

In homogenization methods, the concept of RVE was firstly proposed by Hill (1963) as "*a sample that is the structurally typical of the whole microstructure for a given material, i.e. containing a suffi-ciently large number of heterogeneities, while being small enough to be considered homogeneous from a continuum mechanics viewpoint*". The quantification of RVE size has been problematic until various statistical approaches were proposed in the past two decades (Gusev, 1997; Terada et al., 2000; Kanit et al., 2003; Gitman et al., 2007). Based on several statistical hypotheses, Kanit et al. (2003) proposed a statistical approach to determine the minimal RVE size for a considered property, in which, the RVE size could be associated with a given precision of the estimated overall property and the number of realizations with a given volume size *V*. Practically, it is applicable in order to determine the minimal number of realizations to consider for a given volume size, in order to estimate the effective property with a given precision (Bironeau et al., 2016).

Using this approach, Kanit et al. (2003) studied the RVE sizes of a two-phase 3D Voronoi mosaic for linear elasticity, thermal conductivity and volume fraction, under uniform displacement, traction and periodic boundary conditions (PBC) (Michel et al., 1999). The results showed that the PBC held an advantage of convergence rate of the mean apparent properties in comparison to other boundary conditions, due to the vanishing of boundary layer effects. A slow rate of convergence for the considered properties would yield a large RVE sizes (Dirrenberger et al., 2014). Also considering the large calculation cost in the case of crystal plasticity, it is preferable to rely on PBC in order to optimize the computation strategy, as it was done in other investigations (Pelissou et al., 2009 and Jean et al., 2011).

The statistical method of Kanit et al. (2003) was implemented for the estimation of RVE size, not only for linear mechanical properties and morphological property, but also for plastic properties: Madi et al. (2006) evaluated the RVE size for 2D/3D viscoplastic composite materials. In their study, the macroscopic strain rate of the 2D/3D material was modeled using a Norton flow rule. Based on the von Mises criterion, an apparent viscoplastic parameter P_v^{app} was firstly defined as the coupling of two parameters of the Norton flow rule K and n, i.e. $P_v^{app}=1/K^n$. The authors showed that the value of P_v^{app} converged towards a constant value with an increasing volume of simulation and that the RVE size for P_v^{app} was found to be smaller than the ones for elastic moduli. In the present work, we will rely on this definition of the apparent viscoplastic parameter, as it is adapted for describing the nonlinear behavior of a macroscopically isotropic polycrystalline viscoplastic material.

As a matter of fact, the concept of RVE has often been used in investigations associated with the average mechanical response of 2D and 3D polycrystalline material. The definition of RVE size can stem from finite element meshing considerations or convergence of mean values for a considered property. For instance, Barbe et al. (2001) described the RVE for a cubic polycrystalline mesh as an equilibrium between the number of grains (238) and the average number of integration points per grain (660) attainable within typical computational means. More recently, Sweeney et al. (2015) estimated the energetic parameter of CoCr stent material in high cycle fatigue by averaging in 5 RVEs with 138–140 grains. Cruzado et al. (2017, 2018) simulated the cyclic deformation of metallic alloys with 20 RVEs and a size of 300 grains, which showed an error less than 10% for elastoviscoplastic properties. Similar determination of material RVE size can also be found in Shenoy et al. (2007, 2008), Martin et al. (2014), Gillner and Muñstermann (2017), Teferra and Graham-Brady (2018). In these Refs, RVE size is defined as a few realizations with a few hundred grains which can realize a convergence of mean properties. However, these analyses do not allow for a rigorous statistical definition of the RVE size.

Rather than relying solely on the convergence of mean properties, the method proposed in Kanit et al. (2003) makes use of the rate of convergence of the ensemble variance of the mean properties with respect to the volume size, thus enabling the definition and estimation of a statistical RVE size for each considered property. However, to the knowledge of the authors, no one ever assessed the RVE size for polycrystalline material in the framework of CPFEM with the statistical RVE method.

Additional consideration has to be made regarding the apparent properties to be considered as criteria for RVE size determination in viscoplasticity. The first one should be the definition of intrinsic dissipation within the context of crystal plasticity. Secondly, the definition of the apparent viscoplastic parameter P_v^{app} will be considered in the crystal plasticity framework. Meanwhile, for the crystal plasticity behavior, material heterogeneity is mainly due to the local grain orientation, which can introduce strong stress concentrations, leading to early onset of plasticity. Both grain orientation and the choice of crystal plastic behavior are likely to influence directly the value of RVE size for mechanical properties, as it will be discussed in the paper.

Overall, in this paper, the RVE size of polycrystalline pure copper will be studied in framework of CPFEM. In the following sections, the material behavior and constitutive model are discussed first. Then, the periodic mesh generation and the computational homogenization method are described in detail, alongside with the various loading cases corresponding to the different properties to be considered for estimating the RVE sizes. Results from computation and statistical analysis are then presented and discussed. Calculations for RVE are performed in the last section of the paper, and comparison is made for the different RVE sizes depending on the considered property.

In the following, vectors are underlined face and written in minuscule, e.g. $\underline{x}$. Second-rank are bold and slant face, e.g. $\boldsymbol{x}$ and $\boldsymbol{X}$, and fourth-rank tensors are bold and straight face capitals, e.g. $\mathbf{X}$. Others are scalar.

2. Crystal plasticity constitutive model

The material involved in this paper was pure polycrystalline copper. Both anisotropic crystal elasticity and plasticity were considered for its behavior. The cubic elasticity is characterized by 3 independent elastic constants, taken from Musienko et al. (2007). The crystal plasticity model considered in the present work was introduced and implemented by Meric et al. (1991) and Cailletaud (1992) in the finite element code ZeBuLoN/ZSet.[1] The Meric–Cailletaud model was chosen for its ability to account for kinematic hardening. This model is popular within the crystal plasticity community and has been used in many previous works on computational mechanics for polycrystalline material (Barbe et al., 2001; Cailletaud et al., 2003b; Diard et al., 2005; Gérard et al., 2009).

The model is briefly summarized here. The constitutive relations are defined hereafter:

$$\dot{\gamma}^s = \left\langle \frac{|\tau^s - X^s| - R_0 - R^s}{K} \right\rangle^n sign(\tau^s - X^s) = \dot{v}^s sign(\tau^s - X^s)$$
$$X^s = C\alpha^s; \ \ \dot{\alpha}^s = \dot{\gamma}^s - D\alpha^s\dot{v}^s, \ with \ \alpha^s(t=0) = 0$$
$$R^s = bQ\sum_r h_{sr}q^r = Q\sum_r h_{sr}\left(1 - e^{-bv^r}\right)$$
$$\dot{q}^s = (1 - bq^s)\dot{v}^s = v \cdot e^{-bv^s}$$
$$\boldsymbol{m}^s = \left(\underline{g}^s \otimes \underline{l}^s + \underline{l}^s \otimes \underline{g}^s\right)/2$$
$$\tau^s = \boldsymbol{m}^s : \boldsymbol{\sigma}; \ \ \dot{\boldsymbol{\varepsilon}}^p = \sum_s \dot{\gamma}^s\boldsymbol{m}^s \tag{1}$$

where for polycrystalline pure copper, 12 slip systems are associated with the calculation, i.e. 4 slip planes $\underline{g}^s$ of type {111} and 3 directions of slip $\underline{l}^s$ of type ⟨110⟩, which depend on the Euler angles of the grains. The Schmid tensor $\boldsymbol{m}^s$ is used to compute the resolved shear stress τ^s and the plastic strain rate $\dot{\boldsymbol{\varepsilon}}^p$. For each slip system, the slip rate $\dot{\gamma}^s$ is defined as a power-law function of τ^s. The parameters K and n relate to the sensitivity of materials to the strain rate. v^s represents the accumulated plastic strain for the slip system s. The couples of thermodynamical force and state variable, (X^s,α^s) and (R^s,q^s), respectively are associated with the kinematic and isotropic hardening. A series of material parameters is used to define the kinematic hardening (C, D), and the isotropic hardening (R_0, Q, b). The symmetric interaction matrix h_{sr} describes the effect of slip on system s on the shear resistance of slip system r, as illustrated by Meric et al. (1991). This includes self-hardening $(s=r)$ and latent hardening $(s \neq r)$.

Finally, the material parameters for a high-purity copper, K, n, R_0, Q, b and h_{sr}, are given in Table 1.

3. Computational approach

3.1. Definition of apparent elastic properties

The micromechanical linear elastic behavior at each integration point in the finite element simulation is described by Hooke's law using the fourth-rank linear elasticity tensor $\mathbf{C}$, such that:

$$\boldsymbol{\sigma}(\underline{x}) = \mathbf{C}(\underline{x}) : \boldsymbol{\varepsilon}(\underline{x}) \tag{2}$$

---

[1] ZeBuLon/ZSet: http://www.zset-software.com/.

Table 1
The parameters of pure copper cubic elasticity and plasticity (Musienko et al., 2007).

Elasticity *Cubic*	Flow *Norton*	Isotropic hardening *Nonlinear*	Kinematic hardening *Nonlinear*	Interaction slip h_{sr}*
C11 = 159.3 GPa C12 = 121.9 GPa C44 = 80.9 GPa	$n = 10$ $K = 5$ MPa s$^{1/n}$	$R_0 = 1.8$ MPa $Q = 6$ $b = 15$	$D = 600$ $C = 4500$	$h1 = 1$, $h2 = 4.4$, $h3 = 4.75$, $h4 = 4.75$, $h5 = 4.75$, $h6 = 5$

* *Note:* $h1 = h_{sr}$ (s = r); $h2 = h_{21}$, h_{31}, h_{32}, h_{54}, h_{64}, h_{65}, h_{87}, h_{97}, h_{98}, $h_{11,10}$, $h_{12,10}$, $h_{12,11}$; $h3 = h_{52}$, h_{63}, h_{75}, h_{83}, h_{91}, h_{94}, $h_{10,6}$, $h_{10,8}$, $h_{11,1}$, $h_{11,4}$, $h_{12,2}$, $h_{12,7}$; $h4 = h_{41}$, h_{72}, h_{86}, $h_{10,3}$, $h_{11,9}$, $h_{12,5}$; $h5 = h_{42}$, h_{43}, h_{51}, h_{61}, h_{71}, h_{73}, h_{76}, h_{82}, h_{84}, h_{85}, h_{92}, h_{96}, $h_{10,1}$, $h_{10,2}$, $h_{10,5}$, $h_{10,9}$, $h_{11,3}$, $h_{11,5}$, $h_{11,7}$, $h_{11,8}$, $h_{12,3}$, $h_{12,4}$, $h_{12,6}$, $h_{12,9}$; $h6 = h_{53}$, h_{62}, h_{74}, h_{81}, h_{93}, h_{95}, $h_{10,4}$, $h_{10,7}$, $h_{11,2}$, $h_{11,6}$, $h_{12,1}$, $h_{12,8}$.

For a given volume V, the fourth-rank tensor of apparent moduli $\mathbf{C}^{\mathrm{app}}$ can be defined by the macroscopic relations:

$$\mathbf{\Sigma} = \boldsymbol{\sigma} = \frac{1}{V} \int_V \boldsymbol{\sigma} dV = \mathbf{C}^{\mathrm{app}} : \boldsymbol{E} \tag{3}$$

where $\mathbf{\Sigma}$ and $\boldsymbol{E}$ are the macroscopic stress and strain second-rank tensors.

For an elementary volume V large enough ($V > V_{RVE}$), the apparent properties do not depend on the boundary conditions (Huet, 1990; Sab, 1992) and equal to the effective properties of the considered material, so that:

$$\mathbf{C}^{\mathrm{app}} = \mathbf{C}^{\mathrm{eff}} \tag{4}$$

The following two macroscopic strain conditions $\boldsymbol{E}_\mu$ and $\boldsymbol{E}_k$ were used in the elastic tests, aiming at computing the apparent shear modulus μ^{app} and apparent bulk modulus k^{app}:

$$\boldsymbol{E_\mu} = \begin{bmatrix} 0 & 1/2 & 0 \\ 1/2 & 0 & 0 \\ 0 & 0 & 0 \end{bmatrix}; \boldsymbol{E_k} = \begin{bmatrix} 1/9 & 0 & 0 \\ 0 & 1/9 & 0 \\ 0 & 0 & 1/9 \end{bmatrix} \tag{5}$$

Then the apparent shear and bulk modulus can be defined from the elastic strain energy density for the macroscopic strain given in Eq. (6) using the Hill–Mandel condition (Hill, 1967), such that:

$$k^{app} = \mathbf{\Sigma} : \boldsymbol{E_k} = Tr(\mathbf{\Sigma}) \\ \mu^{app} = \mathbf{\Sigma} : \boldsymbol{E_\mu} = \Sigma_{12} \tag{6}$$

3.2. Definition of apparent plastic property

In this work, the notion of apparent viscoplastic parameter is considered as defined in Madi et al. (2006) for characterizing viscoplasticity. For the concerned polycrystalline copper, two hypotheses are made:

(1) The von Mises criterion is defined for isotropic material behavior. In the present case, although the local material behavior is anisotropic, the macroscopic behavior is considered isotropic, since the grains have been generated with a statistically isotropic distribution of orientation. Therefore, the von Mises criterion is suitable for macroscopic numerical considerations. Based on von Mises criterion, the total plastic deformation is equal to the sum of micro shear deformation on all activated slip systems for each element of volume, as described in the following equations:

$$\dot{e}^p = \mathbf{\Sigma} : \dot{\boldsymbol{E}}^v = \sum_s^{12} \tau^s \dot{\gamma}^s = \bar{\sigma} \cdot \dot{p}, \ \bar{\sigma} = \sqrt{3J_2(S_{ij})} \tag{7}$$

where, $\dot{e}^p$ is the macroscopic plastic energy rate. $\bar{\sigma}$ denotes the equivalent uniaxial tensile stress, which is associated with $J_2(S_{ij})$ the second invariant of the deviatoric part $\boldsymbol{S}_{ij}$ of the macroscopic stress tensor $\mathbf{\Sigma}$. $\boldsymbol{E}^v$ is the macroscopic viscoplastic strain tensor. p is the equivalent accumulated viscoplastic strain. Local quantities, such as the resolved shear stress and plastic slip rate on each slip systems are computed in the local material frame, and then expressed in the macroscopic frame before averaging.

(2) The apparent global plastic strain rate can be also approximated by a simple Norton flow rule:

$$\dot{p} = \left(\frac{\sqrt{3J_2(S_{ij})}}{K^{app}} \right)^{n^{app}} \tag{8}$$

Generally, this assumption can be valid, only if all local materials have the same parameters n and K, as stated by Rougier et al. (1993) in case of creep. The same K and n parameters are used for each slip system in the present work, hence allowing us to rely on Eq. (8) for pure polycrystalline copper.

Combining Eqs. (7) and (8), one can obtain:

$$\dot{e}^p = \mathbf{\Sigma} : \ \dot{\boldsymbol{E}}^v = \sum_s^{12} \tau^s \dot{\gamma}^s = \sqrt{3J_2(S_{ij})} \cdot \left(\frac{\sqrt{3J_2(S_{ij})}}{K^{app}} \right)^{n^{app}} \tag{9}$$

For the sake of comparison, we rely on the concept of apparent viscoplastic parameter P_v^{app} as defined by Madi et al. (2006) for isotropic viscoplastic behavior, such that:

$$P_v^{app} = \frac{1}{K^{app^{n^{app}}}} \tag{10}$$

Then the Eq. (9) becomes:

$$\dot{e}^p = \mathbf{\Sigma} : \ \dot{\boldsymbol{E}}^v = \sum_s^{12} \tau^s \dot{\gamma}^s = P_v^{app} \left(\sqrt{3J_2(S_{ij})} \right)^{n^{app}+1} \tag{11}$$

The procedure for determining P_v^{app} is as follows: for each realization, a uniaxial tensile test is carried out under PBC with prescribed macroscopic strain rate control. As polycrystalline pure copper is a rather strain rate insensitive material at room temperature (Carreker and Hibbard, 1953), only one strain rate of 10^{-3} s^{-1} is considered. The duration of the test is 0.1 s. Therefore, the maximum macro strain is 10^{-4}, which is in the scope of the practical use for the Meric–Cailletaud model (Meric et al., 1991; Cailletaud, 1992). At the end of tensile test, output values ($\sqrt{3J_2(S_{ij})}, \dot{e}^p$) are computed. Using the least square fitting method, the value of P_v^{app} is identified as the coefficient of the fitted power law, as shown in Fig. 1. The best fit is obtained by increasing the volume size: $R^2 \geq 0.9$ for 8gr, 0.92 for 27gr, 0.94 for 64gr, 0.96 for 125gr, 0.98 for 216gr and 0.99 for 343gr, R^2 being the statistical coefficient of determination.

Furthermore, in order to determine the RVE size of polycrystalline copper for viscoplasticity, the intrinsic dissipation energy density during tensile test was also chosen as one plastic property to estimate the RVE size. For each slip system, the intrinsic dissipation power is defined as the plastic power minus the stored power associated with isotropic and kinematic hardening, as proposed by Chrysochoos et al. (1989).

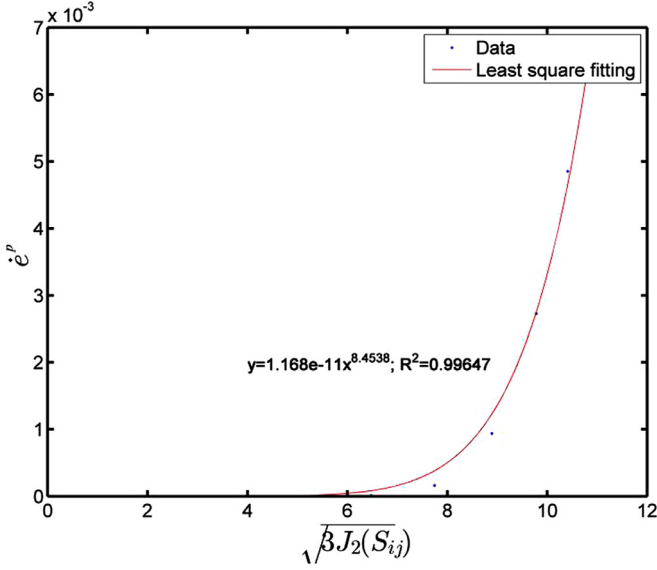$$\dot{d}_1^s = \tau^s \dot{\gamma}^s - X^s \dot{\alpha}^s - R^s \dot{q}^s \tag{12}$$

Fig. 1. A fitting result of $\dot{e}^p$ $vs\sqrt{3J_2(S_{ij})}$, under 343 number of grains; P_v^{app} is $1.168e-11$ and the corresponding values of n^{app} and K^{app} are 7.45 and 29.29, respectively.

The spatially intrinsic dissipation energy density during the tensile test is computed as follows:

$$d_1^{tension} = \int_t \frac{1}{V} \iiint_V \sum_s \dot{d}_1^s dV \, dt \tag{13}$$

3.3. Determination of RVE size

Based on mathematical morphology considerations, for an ergodic stationary random function $Z(x)$, one can compute the ensemble variance $D_Z^2(V)$ of its average value $\bar{Z}(V)$ over the volume V (Matheron, 1971; Cailletaud et al., 1994; Kanit et al., 2003):

$$D_Z^2(V) = D_Z^2\left(\frac{A_3}{V}\right) \tag{14}$$

where D_Z^2 is the point variance of $Z(x)$ in volume V and A_3 is the integral range of the random function $Z(x)$, defined as:

$$A_3 = \frac{1}{D_Z^2} \int_{\mathbb{R}^3} \bar{W}_2(h)dh \tag{15}$$

where h is a two-point segment, and $\bar{W}_2(h)$ is the centered 2nd order correlation function such that, for a prescribed property Z and for $x \in V$:

$$\bar{W}_2(h) = \overline{\left(Z(x+h) - \bar{Z}\right)\left(Z(x) - \bar{Z}\right)} \tag{16}$$

In case of the Voronoi mosaic model, the value of A_3 is determined as a constant of 1.179 given by Gilbert (1962). Using a modified scaling law with exponent γ, as proposed by Lantuéjoul (1990), the variance can be rewritten as follows:

$$D_Z^2(V) = D_Z^2\left(\frac{A_3^*}{V}\right)^\gamma \tag{17}$$

A_3^* is also homogeneous to a volume of material like A_3 and can readily be used to determine RVE sizes. But there is not a direct definition as Eq. (15), anymore.

In the case of a two-phase material, Kanit et al. (2003) assumed that $\bar{Z}$ was equal to the arithmetic average of considered property with Z_1 for phase 1 and Z_2 for phase 2. The point variance D_Z^2 of the random variable Z was given by:

$$D_Z^2 = P(1-P)(Z_1 - Z_2)^2 \tag{18}$$

where P is the volume fraction of phase 1 in volume V. When it comes to polycrystalline material, we can suppose that the microstructure contains a large number of phases, *i.e.* grains. For each phase or grain, the material behavior is different because of the difference of orientation. Eq. (18) can then be extended to multi-phase microstructures, as follows:

$$D_Z^2 = \sum_i^T P_i\left(Z_i - \bar{Z}\right)^2 \tag{19}$$

where T is the number of grains or phase number.

Finally, in order to determine the RVE size, Dirrenberger et al. (2014) reformulated Eq. (17) to reduce the information of D_Z^2 and A_3^*, as follows:

$$D_Z^2(V) = GV^{-\gamma} \tag{20}$$

with $G = D_Z^2 A_3^{*\gamma}$, since A_3^* cannot be deduced independently. Thus only two parameters G and γ are needed to identify from the statistical data obtained by linearization as follows:

$$\log D_Z^2(V) = \log G - \gamma \log V \tag{21}$$

Following the method proposed in Kanit et al. (2003), the relative sampling error in the effective properties arises:

$$\epsilon_{rel} = \frac{2D_Z(V)}{\bar{Z}\sqrt{n}} \Rightarrow \epsilon_{rel}^2 = \frac{4G}{\bar{Z}^2 n V^\gamma} \tag{22}$$

hence yielding the definition of the RVE size, for a given relative error ε_{rel}

$$V_{RVE} = \sqrt[\gamma]{\frac{4G}{\epsilon_{rel}^2 \bar{Z}^2 n}} \tag{23}$$

3.4. Periodic three-dimensional mesh generation

In this paper, a methodology is employed for generating and meshing 3D random polycrystals. The associated mesh optimization approach and statistical work of mesh quality are fully presented in the reference paper by Quey et al. (2011). The corresponding algorithms are implemented and distributed in an open-source software package: Neper.[2] Thanks to the self-contained codes in Neper, the Voronoi tesselation can be constructed with a periodicity constraint, needed for PBC. For the sake of simplicity and comparison with results from the literature (Madi et al., 2006), an isotropic morphological and crystallographic texture is considered. In order to obtain the isotropic distribution of the grain orientation for a periodic sample, the arbitrary shaft points of all crystals in the sample must span uniformly the surface of a sphere, as suggested by Néda et al. (1999). For the sake of achieving the condition, the three Euler angles (α, β, γ) in the $Z–X–Z$ type of each generated grain cell will be given different distribution rules: α and γ are generated randomly with a uniform distribution on $[0, 2\pi]$, while, β is chosen randomly in the range $[0, \pi]$ with a weighted distribution and the weight factor $\sin(\beta)$ should be randomly in the range $[0, 1]$. Afterwards, the microstructure was meshed with linear tetrahedral elements as shown in Fig. 2b. At least 300 elements were used for each grain, which is a reasonable value, considering the usual practice in the full-field simulation literature (Cailletaud et al., 2003a; Roters et al., 2011; Cruzado et al. 2015). The grain size in the generated microstructure follows a normal distribution function with a mean value of 20 μm and a standard deviation of 13.5 μm. Fig. 2c represents an example of equivalent von Mises stress distribution at a macroscopic strain of 0.01%, and the stress within grains microstructure was observed by slicing perpendicularly to Z axis, as shown in Fig. 2d.
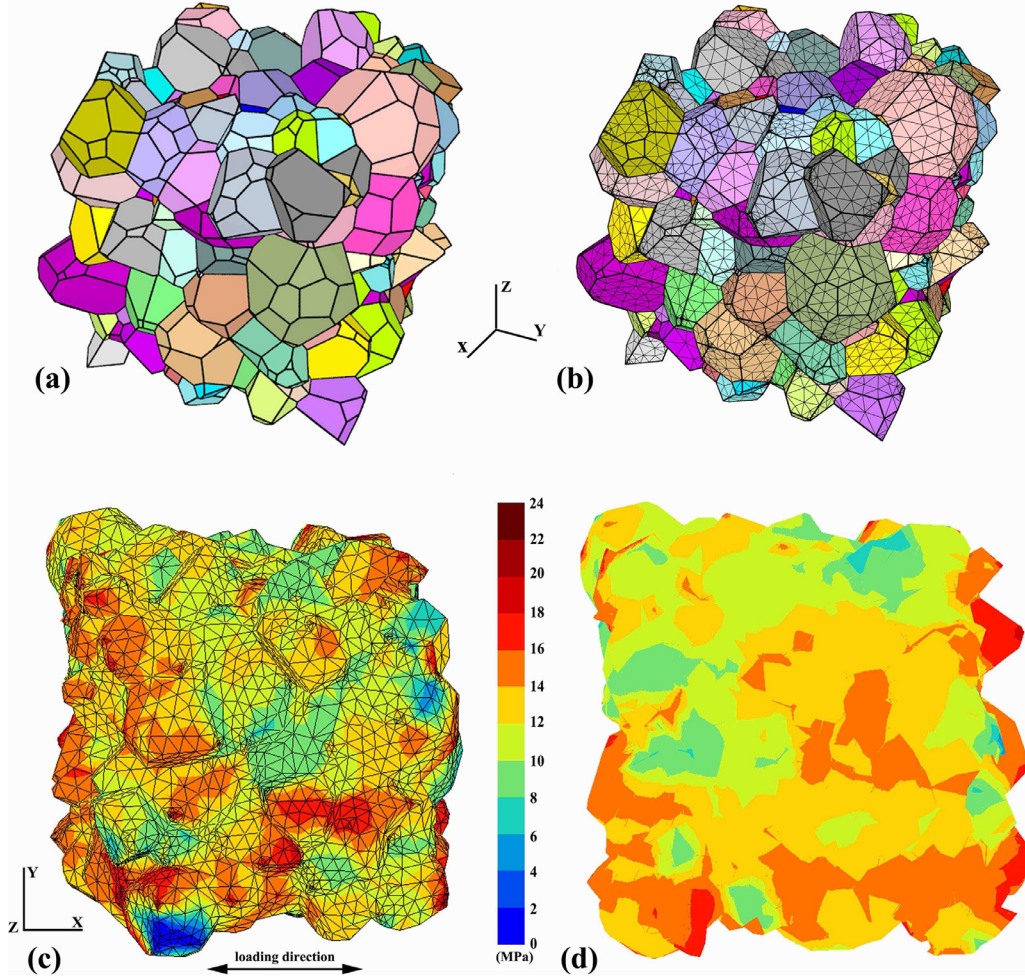
Fig. 2. (a) 3D periodic generation of a polycrystalline sample (343 grains); (b) periodic meshing with tetrahedral elements; (c) The von Mises stress distribution with strain of 0.1% after tensile test; (d) XY workplace of (c) on half Z.

Table 2
Number of realizations N used for all considered domain sizes.

Domain size/Gran number (V)	8	27	64	125	216	343
Mesh generation time	15 s	1.5 min	6 min	13 min	22 min	35 min
Elastic calculation time	1.2 s	3 s	6.7 s	15 s	27 s	42 s
Plastic calculation time	2 min	6.7 min	18 min	37.6 min	97.6 min	194.2 min
Number of realizations for u^{app}	514	140	56	28	16	10
Number of realizations for k^{app}	466	112	41	19	15	10
Number of realizations for $d_1^{tension}$	352	90	40	28	14	8
Number of realizations for P_v^{app}	56	38	26	16	12	6

4. Results and discussion

According to the approach described hereinabove, several realizations were generated for statistical analysis, with different number of grains, ranging from 8 to 343, as listed in Table 2. The generated microstructure has a mean grain size (diameter) of 20 µm. Thus, the actual volume size is directly related to the number of grains. For the sake of simplicity, we used the number of grains in place of the volume size (V). Generally, the number of realizations N should be different for each domain size in order to achieve a similar measurement error for all sizes considered. Using Eq. (22) the measurement error for all domain sizes were controlled at under 1% for elastic properties, under 3% for intrinsic dissipation. On the contrary, the measurement error remains high, just under 120% for apparent viscoplastic parameter P_v^{app}, mostly due to the large intrinsic variability of the property. To accomplish the

generation and meshing of microstructures, a computer equipped with an Intel Core i7-4750HQ CPU @ 2.0 GHz and 8GB RAM was employed. The consumed time of meshing, as well as elastic and plastic calculations for one realization is also presented for reference in Table 2.

4.1. Isotropy of mean apparent moduli

The microstructures used in tensile tests in framework of CPFEM are expected to be macroscopically isotropic. If a small volume element V is considered, it may not exhibit an isotropic behavior. Therefore, it is necessary to check whether the generated polycrystal is isotropic or not. For that purpose, six computations are necessary for finding the 21 components of apparent elastic tensor C^{app} on each realization, using PBC. From averaging all the realizations, the obtained full elastic moduli tensors with the intervals of confidence corresponding to plus and minus two

Table 3
The mean values and variance of components of **C**^{app}.

C^{app} with $V=27$, $N=140$					
$177,772 \pm 21,975$	$83,450 \pm 17,823$	$83,492 \pm 19,330$	150 ± 8234	$-437 \pm 10,666$	$700 \pm 11,035$
–	$176,163 \pm 24,036$	$85,471 \pm 15,358$	$379 \pm 11,011$	218 ± 8101	$282 \pm 13,208$
–	–	$176,090 \pm 24,364$	$969 \pm 12,566$	$385 \pm 11,306$	-174 ± 7793
–	–	–	$48,648 \pm 9537$	-207 ± 7245	287 ± 7467
–	–	–	–	$46,647 \pm 11,579$	10 ± 7240
–	–	–	–	–	$46,723 \pm 10,862$
C^{app} with $V=125$, $N=28$					
$192,435 \pm 10,455$	$95,170 \pm 7999$	$95,911 \pm 6895$	35 ± 4256	467 ± 6260	-667 ± 4638
–	$189,378 \pm 8427$	$98,150 \pm 8934$	187 ± 5717	124 ± 3503	344 ± 5591
–	–	$188,587 \pm 5096$	-555 ± 5096	-580 ± 5366	107 ± 3604
–	–	–	$50,776 \pm 5729$	132 ± 3515	154 ± 3574
–	–	–	–	$48,361 \pm 4418$	94 ± 3864
–	–	–	–	–	$47,623 \pm 4940$
C^{app} with $V=343$, $N=10$					
$195,062 \pm 5184$	$98,622 \pm 4276$	$98,900 \pm 1214$	-217 ± 2640	656 ± 3267	234 ± 3345
–	$193,190 \pm 3821$	$101,367 \pm 3177$	-53 ± 3122	-85 ± 2160	-544 ± 3445
–	–	$192,721 \pm 5921$	1 ± 2780	510 ± 2207	-159 ± 2019
–	–	–	$50,830 \pm 2715$	-146 ± 1824	-212 ± 2358
–	–	–	–	$48,241 \pm 1757$	56 ± 2700
–	–	–	–	–	$48,023 \pm 3837$

standard deviations ($\pm 2D_Z$) are given in Table 3 for different volume sizes (components in MPa). The standard deviation decreases with increasing volume size. The averaged tensor components obtained for 343 grains are characteristic of isotropic elasticity since $\overline{C_{11}} \approx \overline{C_{22}} \approx \overline{C_{33}}$ and $\overline{C_{12}} \approx \overline{C_{13}} \approx \overline{C_{23}}$ with a maximal error of 5%, and $\overline{C_{44}} \approx \overline{C_{55}} \approx \overline{C_{66}}$ are approximately equal to $\frac{\overline{C_{11}} - \overline{C_{22}}}{2}$ with a maximal error of 10%. The remaining components should vanish in the isotropic case, and here, they take up less than 1% of $\overline{C_{11}}$. It can be also observed that the elastic moduli tensor components have not reached their converged values for smaller volumes, which is likely due to a bias of representatively as studied by (Hazanov and Huet, 1994; Huet, 1997; Hazanov, 1998)

4.2. The apparent elastic and plastic properties

After confirming the isotropy of the generated microstructures, elastic properties k^{app} and μ^{app} are investigated, as well as the intrinsic dissipation and the apparent viscoplastic parameter for all realizations. Fig. 3 illustrates the changes of the four apparent parameters with respect to volume size, including mean value and standard deviation. Increasing the volume size, the mean values of μ^{app} and k^{app} increase gradually and stabilize respectively at $49,031 \pm 1085$ MPa and $130,972 \pm 2385$ MPa on the 343 volume size, which are consistent with common values for polycrystalline pure copper. Similar convergence behavior can be observed for $d_1^{tension}$. Its mean value reaches 53 J/m^3 with the corresponding intervals of confidence of 4.3 J/m^3 on the 343 volume size, which is in the same magnitude level as previous studies for metals, such as Chrysochoos and Martin (1989) and Chrysochoos et al. (2009).

The definition of P_v^{app} consists of two parameters, K^{app} and n^{app}. The fluctuation of both parameters may yield a large change of P_v^{app} in magnitude. For better presenting, the order of magnitude $log(P_v^{app})$ was drawn *vs.* the volume size in Fig. 3 as the substitute of P_v^{app}. However, the relative error, floating around 9%, is a little higher than those of elastic properties and intrinsic dissipation because of fewer realizations. When the volume size increases to 343, the fluctuation tends to weaken, and the averaged value of $log(P_v^{app})$ stabilizes at -10.74, with a fluctuation range of ± 0.8. Interestingly, this value is also approximately the combination of the two parameters of the single crystal constitutive law, $K = 5$ and $n = 10$, producing the value of $10^{-10.7}$ as the definition of $P_v = \frac{1}{K^n}$. Considering a large enough volume of polycrystalline pure copper

at the strain rate of 10^{-3} s^{-1}, the following equation can be possibly satisfied:

$$P_v^{app} = \frac{1}{K^{app^{n^{app}}}} = P_v^{eff} = \frac{1}{K^n} \tag{24}$$

Nevertheless, the apparent parameters K^{app} and n^{app} are not necessarily equal to the actual values of K and n for the single crystal behavior law. Here they converge at 29.06 and 7.32 for 343 volume sizes, respectively, with a relative error of about 3% for both K and n.

4.3. Fluctuation of apparent properties and RVE sizes

As specified in Eq. (23), in order to compute RVE sizes, three variables ($D_Z, \bar{Z}, \gamma$) have to be estimated. A linear fitting was done according to Eq. (21) in the logarithm scale for the four properties, as shown in Fig. 4. The slope values of each line corresponds to different values of γ, which are close to 1 for μ^{app}, k^{app} and $d_1^{tension}$. P_v^{app} exhibits a γ value of 4.9 meaning that the defined apparent viscoplastic parameter has a much faster statistical convergence rate than the other investigated properties. The intercept term b can be used to work out the variables, G.

In order to explain the discrepancies observed for γ, the point deviation D_Z in each realization is also computed for the four properties using Eq. (19), and the results are specified in Fig. 5. On 343 volume size, $D_{\mu^{app}}$, $D_{k^{app}}$, and $D_{d_1^{tension}}$ have converged at 11,713, 4774, and 34, with small fluctuations. By normalizing the point deviation D_Z over the converged property $\bar{Z}$ ($D_Z/\bar{Z}$), one can find that the intrinsic dissipation energy has higher inner deviation than the apparent elastic properties (68.4% for $d_1^{tension}$, 3.8% and 23% for k^{app} and μ^{app}, respectively for 343 volume size). For $D_{P_v^{app}}$, this value can reach at over 100, because of the nonlinearity and high sensitivity of this parameter. This implies that the orientation distribution seems to have a stronger impact on the plastic behavior variability in comparison to its effect on elastic properties. Also, it seems that the high γ exponent for $D_{P_v^{app}}^2(V)$ could be correlated with the nonlinearity and sensitivity of the viscoplastic parameter.

One of the advantages of relying on microstructural computation is the ability to consider each grain or phase individually. For this purpose, Fig. 6 illustrates the impact of grain orientation on crystal plasticity, by analyzing the local heterogeneities of the plastic behavior in a realization with 343 grains, including von Mises
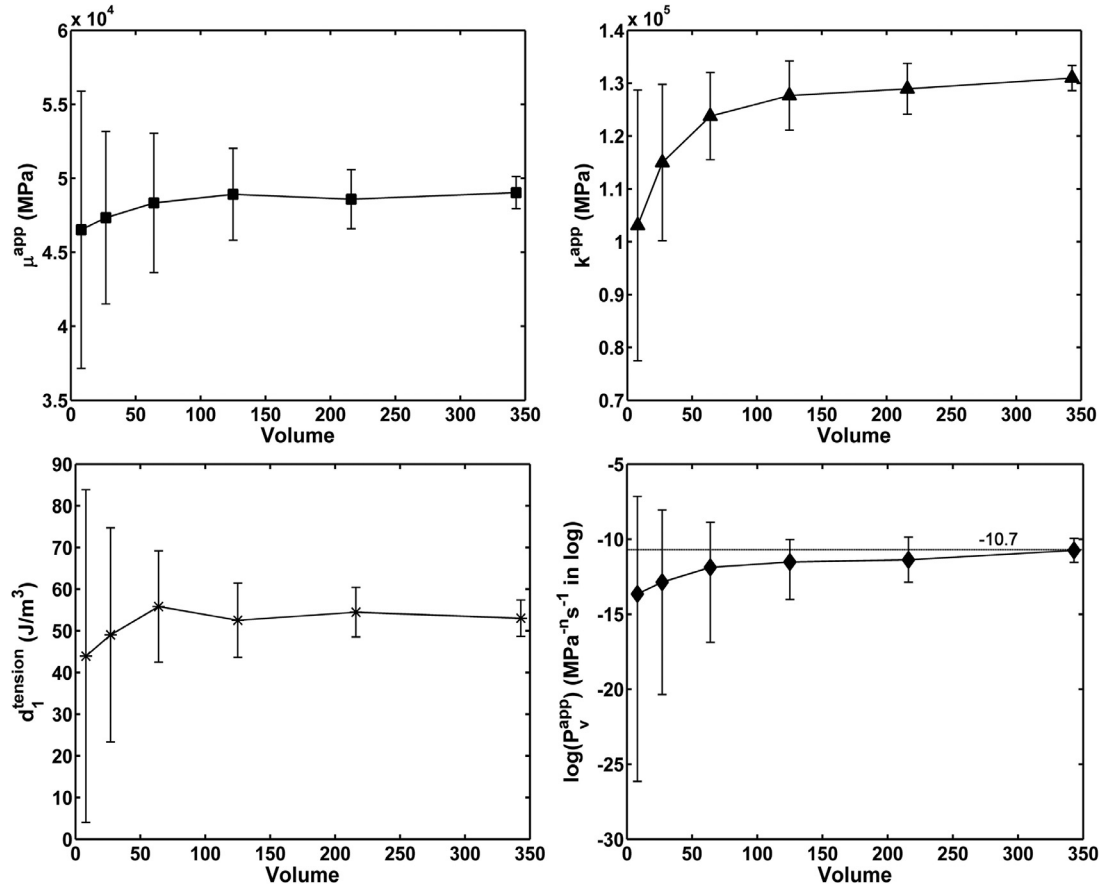
Fig. 3. The mean values and variances for the four apparent properties with increasing volume size. The error bar means plus and minus two standard deviations ($\pm 2D_z$).
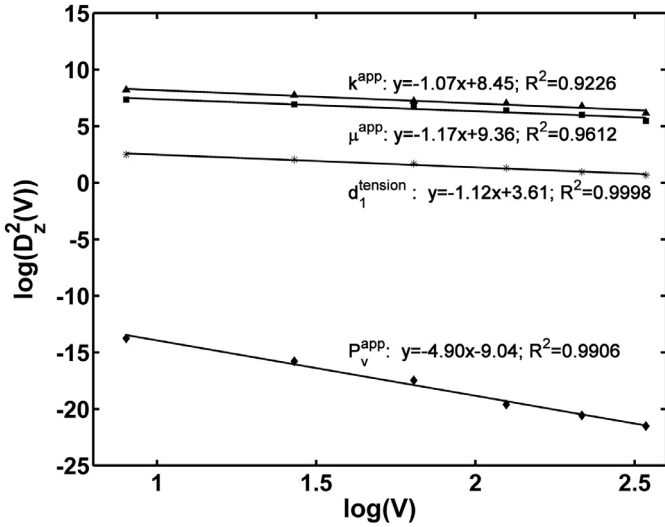

Fig. 4. Linear fitting for variances of four apparent properties *vs.* volume sizes.

Table 4
The associated variables in Eq. (23) for four apparent properties.

Variables	μ^{app}	k^{app}	$d_1^{tension}$	P_v^{app}
γ	1.07	1.17	1.12	4.90
G	2.82E8	2.29E9	4073.80	9.12E$-$10
$\bar{Z}$	49,031.18	130,972.25	53.03	2.19E$-$11

Table 5
RVE sizes estimated from computation with $n = 1$.

Relative error	1%	2%	5%	10%
$V_{\mu^{app}}$	2756	753	135	37
$V_{k^{app}}$	1504	461	96	29
$V_{d_1^{tension}}$	17,894	5190	1010	293
$V_{P_v^{app}}$	2788	2101	1445	1089

stress and plastic energy rate evolution with respect to equivalent macroscopic uniaxial tensile stress. The curves for the two properties were drawn for each grain and the whole volume. As shown in the von Mises curves, grains in the volume hold different equivalent stress, ranging from 6 MPa to 16 MPa. Some grains actually remain in the elastic regime during the tensile test. Meanwhile, grains yield heterogeneous plastic power depending on the grain orientation for the same equivalent macroscopic uniaxial tensile stress, as shown on the right hand side in Fig. 6. These heterogeneities are related to the local grain orientation, local anisotropic elasticity and anisotropic crystal plasticity framework.

Finally, all the associated variables in Eq. (23) for four apparent properties were obtained and listed in Table 4. The minimum domain sizes that are necessary to reach a given precision are finally shown for four apparent properties, in Table 5. In general, for a given material, the RVE size depends on the specific investigated property. For polycrystalline pure copper, as Table 5 shows, the inequality exists: $V_{k^{app}} < V_{\mu^{app}} < V_{d_1^{tension}}$, $V_{P_v^{app}}$. Furthermore, the RVE size for P_v^{app} does not depend too much on the chosen precision, in comparison to the other three properties. In practical use, for a 5% relative error, a volume size of 135 grains can be considered for elastic properties, while for intrinsic dissipation and apparent viscoplastic parameter, the volume sizes must be larger
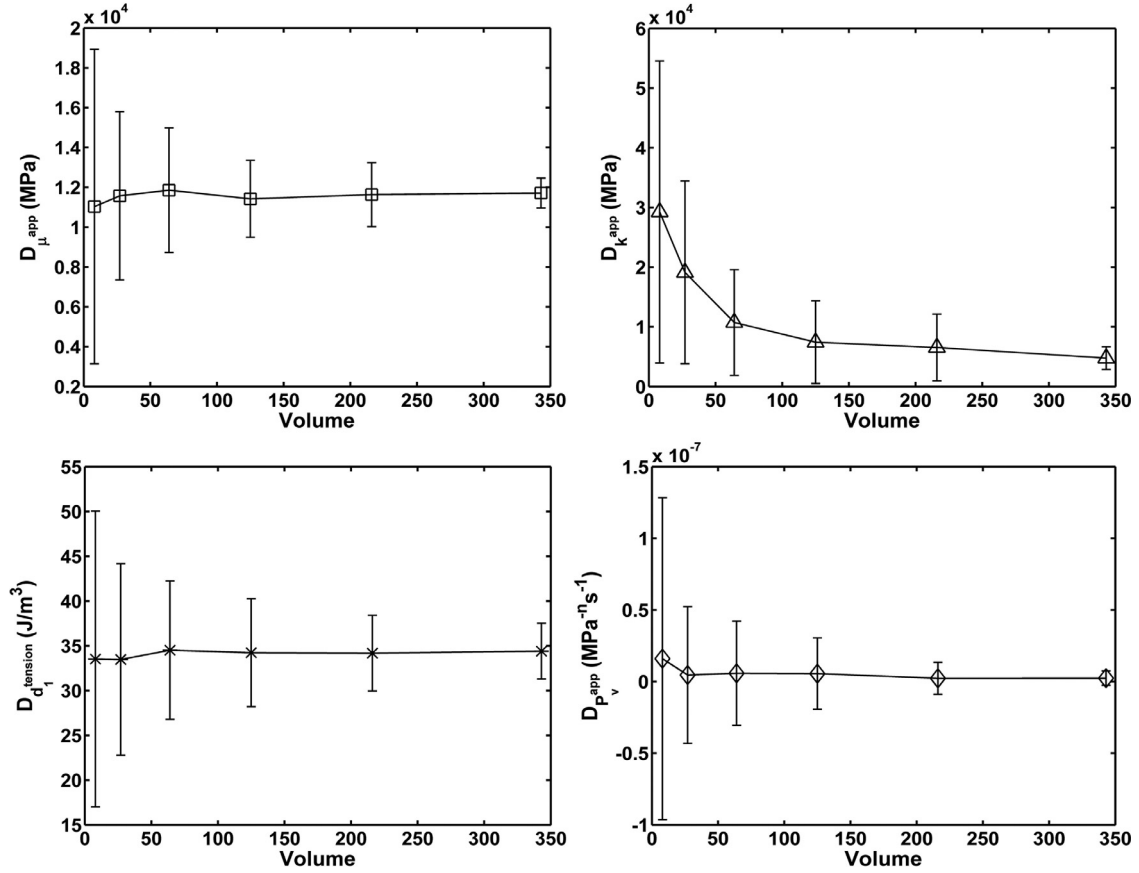
Fig. 5. The point deviation of four apparent properties for each volume size, in which the error bar represents plus and minus two standard deviations on the variance.
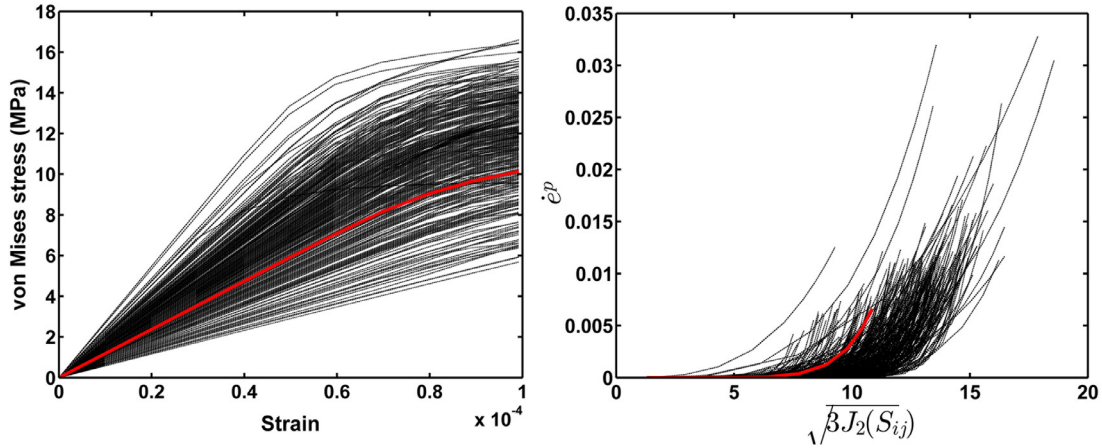

Fig. 6. The heterogeneities of von Mises stress *vs.* macroscopic strain (left) and plastic energy rate evolution with respect to the equivalent uniaxial tensile stress (right) for each grain in one volume with 343 grains (black lines represent each grain; red lines are for the whole volume).

than 1010 grains and 1445 grains, respectively. If a higher precision is required, more realizations can be also considered, such as for a precision of 1% with $n = 50$ realizations, $V_{\mu^{app}}^{RVE} = 71$, $V_{k^{app}}^{RVE} = 54$, $V_{d_1^{tension}}^{RVE} = 545$ and $V_{P_v^{app}}^{RVE} = 1254$.

However, in the case of isotropic plasticity behavior, the RVE size for the same property P_v^{app} used by Madi et al. (2006) was found smaller than for the isotropic elastic ones. A different conclusion in the present results is likely due to the difference of material behavior, *i.e.* anisotropic elasticity and crystal plasticity. As discussed before about the deviation D_Z, crystal plasticity highly depends on the grain orientation, as different activated

slip systems produce different plastic deformations. The effect of anisotropic elasticity appears to yield lower statistical heterogeneity than the crystal plasticity behavior, *i.e.* yielding a smaller RVE size in comparison.

Based on Fig. 6, it appears that plastic deformation takes place in most grains during the tensile test, but localization operates in only a minority of grains, *i.e.* less than 10% of them. This plastic strain localization and stress concentration phenomenon could explain a high γ exponent for $D_{P_v^{app}}^2(V)$. As a matter of fact, a pattern of localization will form for any number of grains due to the morphological and material anisotropies. Therefore, a large number of grains is not needed for ensemble variance convergence on

the averaged value of the viscoplastic parameter. Results from Eq. (23) and Table 5 might lead to another conclusion: the RVE size for P_v^{app} is rather large and only decreases slowly with increasing the relative error. This is due to the high intrinsic point variance of P_v^{app}, *i.e.* G in Eq. (22). This variability is related to the nonlinear nature of the localization phenomena. This large point variance counterbalances the effect of a fast ensemble variance convergence. One could argue that the point variance of P_v^{app} is likely to be related to a strong material heterogeneity as induced in the present work by elastic anisotropy and crystal plasticity.

5. Conclusions and prospects

Aiming at computing the intrinsic dissipation of pure copper based on a crystal plasticity framework, virtual polycrystalline samples were generated based on EBSD microstructural analysis, and the RVE size for various mechanical properties was estimated. A statistical analysis method was used to determine the RVE size of polycrystalline pure copper for four properties, including two isotropic elastic properties: shear and bulk modulus, the viscoplastic parameter and the intrinsic dissipation energy density during a tensile test. The main conclusions are listed below:

1. The statistical RVE method developed by Kanit et al. (2003), is applicable to viscoplastic polycrystalline materials modeled within a crystal plasticity finite element framework.
2. RVE sizes obtained are smaller for elastic properties than for plastic properties, likely due to the anisotropic elastoviscoplastic model chosen for the material behavior, as well as the polycrystalline nature of the samples, both inducing stronger heterogeneities in the mechanical fields. This conclusion is opposite to the ones made by Madi et al. (2006), while considering an isotropic elastoplastic biphasic material.
3. The computational microstructural study allowed to characterize the local heterogeneities associated with plasticity, hence giving an insight on the microstructural behavior explaining the statistical macroscopic trends observed.
4. The viscoplastic parameter is related to the nonlinear phenomenon of plastic localization, inducing strong local variability for P_v. This inherent intrinsic heterogeneity leads to a high point variance, which itself will invariably yield larger RVE size in comparison to linear properties.

The statistical analysis provided in this paper can be applied to other polycrystalline materials for various properties, given that a microstructural morphological model is available for generating a virtual statistical population of samples. Introducing more information about the microstructure of materials appears as a necessity for improving the predictive capability of such statistical techniques. Further work will involve the extension of the present approach to the fatigue of metallic polycrystalline materials. The fatigue strength of polycrystalline materials is a longstanding problem in mechanical design, especially in the very high cycle fatigue regime, where the stress level is much lower than traditional fatigue limit (Bathias and Paris, 2004; Stanzl-Tschegg et al., 2007; Phung et al., 2014; Torabian et al., 2016a, 2016b, 2017a, 2017b). In order to reduce experiment duration time, many authors have resorted to the method of self-heating tests, in which the thermomechanical response of the material during cyclic loading is analyzed and the intrinsic dissipation is taken as the fatigue damage indicator to evaluate fatigue strength at various stress levels in the high and very high cycles fatigue domain (Luong 1995; La Rosa et Risitano 2000; Boulanger et al., 2004; Doudard et al., 2010; Chrysochoos et al., 2008; Connesson et al., 2011; Blanche et al., 2015; Guo et al., 2015). Physically, coming from the irreversibility of the plastic deformation, intrinsic dissipation is assumed to be related to the microplastic deformation in gigacycle fatigue regime,

i.e. the crystal slipping behavior at the grain scale. The approach developed in the present work could thus be used to determine the RVE size associated with intrinsic dissipation during very-high cycle fatigue. Relying on full-field crystal plasticity finite element analysis could thus further our understanding of the damage phenomena taking place at the microscale.

Acknowledgments

References

Barbe, F., Decker, L., Jeulin, D., Cailletaud, G., 2001. Intergranular and intragranular behavior of polycrystalline material. Part 1: FE model. Int. J. Plasticity 17, 513–536.

Bathias, C., Paris, P.C., 2004. Gigacycle Fatigue in Mechanical Practice, vol. 185. CRC Press.

Bironeau, A., Dirrenberger, J., Sollogoub, C., Miquelard-Garnier, G., Roland, S., 2016. Evaluation of morphological representative sample sizes for nanolayered polymer blends. J. Microsc. 264, 48–58.

Blanche, A., Chrysochoos, A., Ranc, N., Favier, V., 2015. Dissipation assessments during dynamic very high cycle fatigue tests. Exp. Mech. 55, 699–709.

Boulanger, T., Chrysochoos, A., Mabru, C., Galtier, A., 2004. Calorimetric analysis of dissipative and thermoelastic effects associated with the fatigue behavior of steels. Int. J. Fatigue 26, 221–229.

Cailletaud, G., Jeulin, D., Rolland, P., 1994. Size effect on elastic properties of random composites. Eng. Comput. 11, 99–110.

Cailletaud, G., 1992. A micromechanical approach to inelastic behaviour of metals. Int. J. Plasticity 8, 55–73.

Cailletaud, G., Chaboche, J.L., Forest, S., Remy, L., 2003a. On the design of single crystal turbine blades. Revue de Metallurgie 165–172.

Cailletaud, G., Forest, S., Jeulin, D., Feyel, F., Galliet, I., Mounoury, V., Quilici, S, 2003b. Some elements of microstructural mechanics. Comput. Mater. Sci. 27, 351–374.

Carreker, R.P., Hibbard Jr., W.R., 1953. Tensile deformation of high-purity copper as a function of temperature, strain rate and grain size. Acta Metall. 1, 656–663.

Chrysochoos, A., Berthel, B., Latourte, F., Pagano, S., Wattrisse, B., Weber, B., 2008. Local energy approach to steel fatigue. Strain 44, 327–334.

Chrysochoos, A., Martin, G., 1989. Tensile test microcalorimetry for thermomechanical behaviour law analysis. Mater. Sci. Eng. A 108, 25–32.

Chrysochoos, A., Wattrisse, B., Muracciole, J.M., Kaim, Y.E., 2009. Fields of stored energy associated with localized necking to steel. J. Mech. Mater. Struct. 4, 245–262.

Chrysochoos, A., Maisonneuve, O., Martin, G., Caumon, H., Chezeaux, J.C., 1989. Plastic and dissipated work and stored energy. Nucl. Eng. Des. 114, 323–333.

Connesson, N., Maquin, F., Pierron, F., 2011. Experimental energy balance during the first cycles of cyclically loaded specimens under the conventional yield stress. Exp. Mech. 51, 23–44.

Cruzado, A., Gan, B., Jiménez, M., Barba, D., Ostolaza, K., Linaza, A., Molina-Aldareguia, J.M., Llorca, J., Segurado, J., 2015. Multiscale modeling of the mechanical behavior of IN718 superalloy based on micropillar compression and computational homogenization. Acta Materialia 98, 242–253.

Cruzado, A., LLorca, J., Segurado, J., 2017. Modeling cyclic deformation of inconel 718 superalloy by means of crystal plasticity and computational homogenization. Int. J. Solids Struct. 122–123, 148–161.

Cruzado, A., Lucarini, S., LLorca, J., Segurado, J., 2018. Microstructure-based fatigue life model of metallic alloys with bilinear Coffin-Manson behavior. Int. J. Fatigue 107 (2018), 40–48.

Diard, O., Leclercq, S., Rousselier, G., Cailletaud, G., 2005. Evaluation of finite element based analysis of 3d multicrystalline material plasticity: application to crystal plasticity model identification and the study of stress and strain fields near grain boundaries. Int. J. Plasticity 21, 691–722.

Dirrenberger, J., Forest, S., Jeulin, D., 2014. Towards gigantic RVE sizes for 3D stochastic fibrous networks. Int. J. Solids Struct. 51, 359–376.

Doudard, C., Calloch, S., Hild, F., Roux, S., 2010. Identification of heat source fields from infrared thermography: determination of 'self-heating' in a dual-phase steel by using a dog bone sample. Mech. Mater. 42, 55–62.

Gérard, C., N'Guyen, F., Osipov, N., Cailletaud, G., Bornert, M., Caldemaison, D., 2009. Comparison of experimental results and finite element simulation of strain localization scheme under cyclic loading. Comput. Mater. Sci. 46, 755–760.

Gilbert, E.N., 1962. Random subdivisions of space into crystals. Ann. Math. Stat. 33, 958–972.

Gillner, K., Münstermann, S., 2017. Numerically predicted high cycle fatigue properties though representative volume elements of the microstructure. Int. J. Fatigue 105, 219–234.

Gitman, I.M., Askes, H., Sluys, L.J., 2007. Representative volume: Existence and size determination. Eng. Fract. Mech. 74, 2518–2534.

Guo, Q., Guo, X., Fan, J., Syed, R., Wu, C., 2015. An energy method for rapid evaluation of high cycle fatigue parameters based on intrinsic dissipation. Int. J. Fatigue 80, 136–144.

Gusev, A., 1997. Representative volume element size for elastic composites: a numerical study. J. Mech. Phys. Solids 45, 1449–1459.

Hazanov, S., 1998. Hill condition and overall properties of composites. Arch. Appl. Mech. 68, 385–394.

Hazanov, S., Huet, C., 1994. Order relationships for boundary conditions effect in heterogeneous bodies smaller than the representative volume. J. Mech. Phys. Solids 42, 1995–2011.

Hill, R., 1967. The essential structure of constitutive laws for metal composites and polycrystals. J. Mech. Phys. Solids 15, 79–95.

Hill, R., 1963. Elastic properties of reinforced solids: some theoretical principles. J. Mech. Phys. Solids 11, 357–372.

Huet, C., 1990. Application of variational concepts to size effects in elastic heterogeneous bodies. J. Mech. Phys. Solids 38, 813–841.

Huet, C., 1997. An integration micromechanics and statistical continuum thermodynamics approach for studying the fracture behavior of microcracked heterogeneous materials with delayed response. Eng. Fract. Mech. 58, 459–556.

Jean, A., Willot, F., Cantournet, S., Forest, S., Jeulin, D., 2011. Large-scale computations of effective elastic properties of rubber with carbon black fillers. Int. J. Multiscale Comput. Eng. 9 (3), 271–303.

Kanit, T., Forest, S., Galliet, I., Mounoury, V., Jeulin, D., 2003. Determination of the size of the representative volume element for random composites: statistical and numerical approach. Int. J. Solids Struct. 40, 3647–3679.

La Rosa, G., Risitano, A., 2000. Thermographic methodology for rapid determination of the fatigue limit of materials and mechanical components. Int. J. Fatigue 22, 65–73.

Lantuéjoul, C.H., 1990. Ergodicity and integral range. J. Microsc. 161, 387–403.

Luong, M., 1995. Infrared thermographic scanning of fatigue in metals. Nucl. Eng. Des. 158, 363–376.

Madi, K., Forest, S., Jeulin, D., Boussuge, M., 2006. Estimating RVE sizes for 2D/3D viscoplastic composite material. Matériaux 2006, Dijon, France. xx, 12 p., 2006. <hal-00144481>

Martin, G., Ochoa, N., Saï, K., Hervé-Luanco, E., Cailletaud, G., 2014. A multiscale model for the elastoviscoplastic behavior of Directionally Solidified alloys: application to FE structural computations. Int. J. Solids Struct. 51 (5), 1175–1187.

Matheron, G., 1971. The Theory Of Regionalized Variables and its Applications, vol. Fascicule 5 of Les Cahiers du Centre de Morphologie Mathématique de Fontainebleau. Ecole des Mines de Paris.

Meric, L., Poubanne, P., Cailletaud, G., 1991. Single crystal modeling for structural calculations. Part 1: model presentation. J. Engng. Mat. Technol. 113, 162–170.

Michel, J.-C., Moulinec, H., Suquet, P., 1999. Effective properties of composite materials with periodic microstructure: a computational approach. Comput. Meth. Appl. Mech. Eng. 172, 109–143.

Musienko, A., Tatschl, A., Schmidegg, K., Kolednik, O., Pippan, R., Cailletaud, G., 2007. Three-dimensional finite element simulation of a polycrystalline copper specimen. Acta Mater. 55, 4121–4136.

Néda, Z., Florian, R., Brechet, Y., 1999. Reconsideration of continuum percolation of isotropically oriented sticks in three dimensions. Phys. Rev. E 59, 3717–3719.

Pelissou, C., Baccou, J., Monerie, Y., Perales, F., 2009. Determination of the size of the representative volume element for random quasi-brittle composites. Int. J. Solids Struct. 46, 2842–2855.

Phung, N.L., Favier, V., Ranc, N., Vales, F., Mughrabi, H., 2014. Very high cycle fatigue of copper: evolution, morphology and locations of surface slip markings. Int. J. Fatigue 63, 68–77.

Quey, R., Dawson, P.R., Barbe, F., 2011. Large-scale 3D random polycrystals for the finite element method: generation, meshing and remeshing. Comput. Methods Appl. Mech. Engrg. 200, 1729–1745.

Robert, C., Saintier, N., Palin-Luc, T., Morel, F., 2012. Micro-mechanical modelling of high cycle fatigue behaviour of metals under multiaxial loads. Mech. Mater. 55, 112–129.

Roters, F., Eisenlohr, P., Bieler, T.R., Raabe, D., 2011. Crystal Plasticity Finite Element methods: in Materials Science and Engineering. John Wiley & Sons.

Rougier, Y., Stolz, C., Zaoui, A., 1993. Représentation spectrale en viscoélasticité linéaire des matériaux hétérogènes. Comptes. Rendus de l'Académie des Sciences Série II 316, 1517–1522.

Sab, K., 1992. On the homogenization and the simulation of random materials. Eur. J. Mech., A/Solids 11, 585–607.

Shenoy, M., Tjiptowidjojo, Y., McDowell, D., 2008. Microstructure-sensitive modeling of polycrystalline IN 100. Int. J. Plast. 24 (10), 1694–1730.

Shenoy, M., Zhang, J., Mcdwell, D.L., 2007. Estimating fatigue sensitivity to polycrystalline Ni-base superalloy microstructures using a computational approach. Fatigue Fract. Eng. Mater. Struct. 30, 889–904.

Stanzl-Tschegg, S., Mughrabi, H., Schoenbauer, B., 2007. Life time and cyclic slip of copper in the VHCF regime. Int. J. Fatigue 29, 2050–2059.

Sweeney, C.A., O'Brien, B., Dunne, F.P.E., McHugh, P.E., Leen, S.B., 2015. Micro-scale testing and micromechanical modelling for high cycle fatigue of CoCr stent material. J. Mech. Behav. Biomed. Mater. 46, 244–260.

Teferra, K., Graham-Brady, L., 2018. A random field-based method to estimate convergence of apparent properties in computational homogenization. Comput. Methods Appl. Mech. Engrg. 330, 253–270.

Terada, K., Hori, M., Kyoya, T., Kikuchi, N., 2000. Simulation of the multi-scale convergence in computational homogenization approaches. Int. J. Solids Struct. 37, 2285–2311.

Torabian, N., Favier, V., Dirrenberger, J., Adamski, F., Ziaei-Rad, S., Ranc, N., 2017a. Correlation of the high and very high cycle fatigue response of ferrite based steels with strain rate-temperature conditions. Acta Mater. 134, 40–52.

Torabian, N., Favier, V., Ziaei-Rad, S., Adamski, F., Dirrenberger, J., Ranc, N., 2016a. Self-Heating Measurements for a Dual-Phase Steel under Ultrasonic Fatigue Loading for stress amplitudes below the conventional fatigue limit. Proc. Struct. Eng. 2, 1191–1198.

Torabian, N., Favier, V., Ziaei-Rad, S., Dirrenberger, J., Adamski, F., Ranc, N., 2016b. Thermal response of DP600 dual-phase steel under ultrasonic fatigue loading. Mater. Sci. Eng. 677, 97–105.

Torabian, N., Favier, V., Ziaei-Rad, S., Dirrenberger, J., Adamski, F., Ranc, N., 2017b. Calorimetric studies and self-heating measurements for a dual-phase steel under ultrasonic fatigue loading. Fatigue and Fracture Test Planning, Test Data Acquisitions and Analysis. ASTM International.